ATP-based therapy prevents vascular calcification and extends longevity in a mouse model of Hutchinson–Gilford progeria syndrome

Ricardo Villa-Bellosta[a,1]

[a]Fundación Instituto de Investigación Sanitaria, Fundación Jiménez Díaz, Universidad Autónoma de Madrid, 28040 Madrid, Spain

Edited by Robert Nussbaum, Invitae, San Francisco, CA, and accepted by Editorial Board Member Christine E. Seidman October 10, 2019 (received for review June 26, 2019)

Pyrophosphate deficiency may explain the excessive vascular calcification found in children with Hutchinson–Gilford progeria syndrome (HGPS) and in a mouse model of this disease. The present study found that hydrolysis products of ATP resulted in a <9% yield of pyrophosphate in wild-type blood and aortas, showing that eNTPD activity (ATP → phosphate) was greater than eNPP activity (ATP → pyrophosphate). Moreover, pyrophosphate synthesis from ATP was reduced and pyrophosphate hydrolysis (via TNAP; pyrophosphate → phosphate) was increased in both aortas and blood obtained from mice with HGPS. The reduced production of pyrophosphate, together with the reduction in plasma ATP, resulted in marked reduction of plasma pyrophosphate. The combination of TNAP inhibitor levamisole and eNTPD inhibitor ARL67156 increased the synthesis and reduced the degradation of pyrophosphate in aortas and blood ex vivo, suggesting that these combined inhibitors could represent a therapeutic approach for this devastating progeroid syndrome. Treatment with ATP prevented vascular calcification in HGPS mice but did not extend longevity. By contrast, combined treatment with ATP, levamisole, and ARL67156 prevented vascular calcification and extended longevity by 12% in HGPS mice. These findings suggest a therapeutic approach for children with HGPS.

vascular calcification | Hutchinson–Gilford progeria syndrome | ATP | pyrophosphate | aging

Hutchinson–Gilford progeria syndrome (HGPS) is an extremely rare sporadic genetic disorder in children, characterized by premature aging and accelerated cardiovascular disease, including vascular stenosis and excessive vascular calcification (1–4). HGPS patients live to a mean age of 13–14 y (range, 8–21 y) (5). Most carry a noninherited autosomal dominant de novo heterozygous mutation of the LMNA gene (c.1824C > T; GGC > GCT; p.G608G) (6, 7). This mutation activates a cryptic splice donor site, resulting in the synthesis of a lamin A mutant, known as progerin, which disrupts the nuclear membrane architecture and causes multiple cellular alterations, including abnormal gene transcription and signal transduction.

The molecular mechanism leading to vascular calcification in HGPS was analyzed in $Lmna^{G609G/+}$ knock-in mice (8), which showed a profound deficiency in extracellular pyrophosphate, a potent inhibitor of vascular calcification (9, 10). Treatment with exogenous pyrophosphate reduced vascular calcification but did not increase the life span of these HGPS mice (8).

Extracellular pyrophosphate availability in HGPS mice may be increased by modifying extracellular pyrophosphate metabolism. Pyrophosphate is enzymatically degraded to phosphate by tissue nonspecific alkaline phosphatase (TNAP) in extracellular fluids (9). Over-expression of TNAP causes vascular calcification (11, 12), which can be prevented by alkaline phosphatase inhibitors (12–14). Moreover, extracellular pyrophosphate is synthesized by the enzyme ectonucleotide pyrophosphatase/phosphodiesterase (eNPP), which hydrolyzes extracellular ATP to generate pyrophosphate and AMP (9). In vascular smooth muscle cells and aortas, eNPP1 is the main source of extracellular pyrophosphate (11). Mutations in eNPP1 result in generalized arterial calcification of infancy, which is characterized by excess calcification of the internal elastic lamina of large and medium-size arteries (15). Moreover, eNPP1-null mice develop ectopic artery calcification (16). Ectonucleoside triphosphate diphosphohydrolase (eNTPD), a direct competitor of eNPP for ATP, is the main enzyme that hydrolyzes ATP to phosphate in vascular smooth muscle cells and aortas (17). Loss of eNTPD activity could increase the availability of ATP for pyrophosphate production by eNPP. Therefore, both the eNPP/eNTPD activity ratio and TNAP activity play key roles in pyrophosphate availability. Therefore, loss of eNTPD and TNAP activities could increase the pyrophosphate production, prevent vascular calcification, and extend longevity in this devastating progeroid syndrome.

Methods

Mice. Male $Lmna^{G609G/+}$ and wild-type littermates were used. The protocol was approved by the ethics committees of the Fundación Instituto de Investigación Sanitaria (FIIS), the Fundación Jiménez Díaz (FJD), and the Madrid Community (PROEX 177/15), and conformed to directive 2010/63EU and recommendation 2007/526/EC regarding the protection of animals used for experimental and other scientific purposes, enforced in Spain under RD1201/2005.

Aorta Isolation and Calcification Assays. Mice aged 30–32 wk were euthanized by carbon dioxide inhalation, and their thoracic aorta tissue was perfused with saline and removed as described (18). For calcification assays, aortas were cultured ex vivo (37 °C, 5% CO_2) in Minimum Essential Medium Eagle

Significance

Hutchinson–Gilford progeria syndrome (HGPS) is an extremely rare sporadic genetic disorder in children characterized by premature aging and accelerated cardiovascular disease, including vascular calcification. The molecular mechanism leading to vascular calcification in HGPS was analyzed in a mouse model of progeria, which showed a profound deficiency in extracellular pyrophosphate, a potent inhibitor of vascular calcification. This study showed that a treatment strategy focused on improving extracellular pyrophosphate metabolism could constitute an alternative therapy against this devastating syndrome and other diseases with pyrophosphate deficiency.

Author contributions: R.V.-B. designed research, performed research, contributed new reagents/analytic tools, analyzed data, and wrote the paper.

The author declares no competing interest.

This article is a PNAS Direct Submission. R.N. is a guest editor invited by the Editorial Board.

Data deposition: The data that support the findings of this study are available in figshare, https://figshare.com/, reference no. 10.6084/m9.figshare.9978794.

[1]Email: metabol@hotmail.com.

This article contains supporting information online at www.pnas.org/lookup/suppl/doi:10.1073/pnas.1910972116/-/DCSupplemental.

First published November 5, 2019.

(MEM; Gibco) containing calcium-45 as a radiotracer (Perkin-Elmer), 1 mmol/L L-glutamine, 100 IU/mL penicillin, 100 μg/mL streptomycin, and 0.1% FBS. Culture medium was replaced daily. After 10 d, the aortas were dried and weighed, and radioactivity was measured by liquid scintillation counting (Perkin-Elmer Tri-Carb 2810TR).

Blood Collection. Blood was obtained from 30 to 32-wk-old mice in heparin-containing tubes. Plasma was separated from cell components (erythrocytes, leukocytes, and platelets) by centrifugation at 5000 × g for 10 min, 4 °C. The blood cell components were washed 5 times with buffer containing 9 g/L NaCl.

Pyrophosphate Metabolism. VSMCs or aortas were incubated ex vivo in Hank's Balanced Salt Solution (HBSS, BE10-527F, Lonza) containing the indicated amounts of pyrophosphate and ^{32}PPi or ATP and [γ^{32}P]ATP (Perkin-Elmer) (17). After the indicated times, ATP and pyrophosphate were separated from orthophosphate, as described (11, 17). Briefly, 20 μL of sample was mixed with 400 μL of ammonium molybdate to bind the orthophosphate (Sigma-Aldrich) and 0.75 mol/L sulfuric acid (Sigma-Aldrich) (19), followed by extraction with 800 μL of isobutanol/petroleum ether (4:1; Sigma-Aldrich) to separate phosphomolybdate from pyrophosphate and ATP. A 400 μL aliquot of each organic phase containing phosphomolybdate was removed, and its radioactivity was counted (19). The same aortas were used for both the ATP and pyrophosphate hydrolysis assays. After the ATP hydrolysis assays, the rings were washed 5 times in HBSS before performing the pyrophosphate hydrolysis assay. Finally, the aortic rings were dried and weighed.

To analyze the products released during ATP hydrolysis, blood or aortas were incubated in HBSS containing ATP and [γ^{32}P]ATP at final concentrations of 1 μmol/L and 10 μCi/mL, respectively (19). After the indicated times, the production of ^{32}Pi and ^{32}PPi was determined by chromatography on PEI-cellulose plates (50488-25EA-F; Sigma-Aldrich) developed with 650 mmol/L K_2HPO_4 (Sigma-Aldrich), at pH 3.0, as described (19). The spots were excised and subjected to liquid scintillation counting (UltraGold, 6013329, Perkin-Elmer) (19).

eNPP, eNTPD, and Phosphatase Activities. eNTPD activity was measured by quantification of ^{32}Pi released by hydrolysis of ATP (1 μmol/L and 10 μCi/mL [γ^{32}P]ATP as a radiotracer), and extracted by the above isobutanol/petroleum method (19). Phosphatase and eNPP activities were measured by assessing the hydrolysis of *p*-nitrophenylphosphate (pNPP; Sigma) and thymidine 5′-monophosphate nitrophenyl (TMPpNP; Sigma). Activity assays were performed in HBSS.

Real-Time PCR. Total RNA was isolated by TRIzol extraction (Invitrogen), and cDNA was generated using the SuperScript III cDNA synthesis system (Invitrogen) according to the manufacturer's instructions (17, 20). Mouse TNAP, eNTPD1, and eNPP1 mRNAs were quantified by real-time PCR using SYBR Green, according to the manufacturer's instructions. All reactions were performed in triplicate. The primers used for amplification were as follows (20): 1) Enpp1 (NM_008813): 5′-GGATTGTGCCAATAAGGACT-3′ (forward), 5′-CAAGAACTGT-TGCTGCTGGAG-3′ (reverse); 2) TNAP (NM_007431): 5′-CTATGTCTGGAACCG-CACTGA-3′ (forward), 5′-AGCCTTTGAGGTTTTTGGTCA-3′ (reverse); and 3) Entpd1 (NM_009848): 5′-AGCCTCCACACAGATCACCTT-3′ (forward), 5′-GCCACCA-CTTGAAACCTGAAT-3′ (reverse). Expression was quantified by the comparative C_T method, with correction for the expression of the endogenous control gene, acidic ribosomal phosphoprotein P0 (RPLP0, accession number: NM_007475).

In Vivo Treatments. Mice were intraperitoneally injected every 2 d with ATP (5 mg/kg; Sigma), alone or in combination with levamisole (0.2 mg/kg; Sigma) and ARL67156 trisodium salt (0.1 mg/kg; 1283, Tocris). Control mice were intraperitoneally injected with saline. Mice were treated from 8 wk of age until death or euthanasia.

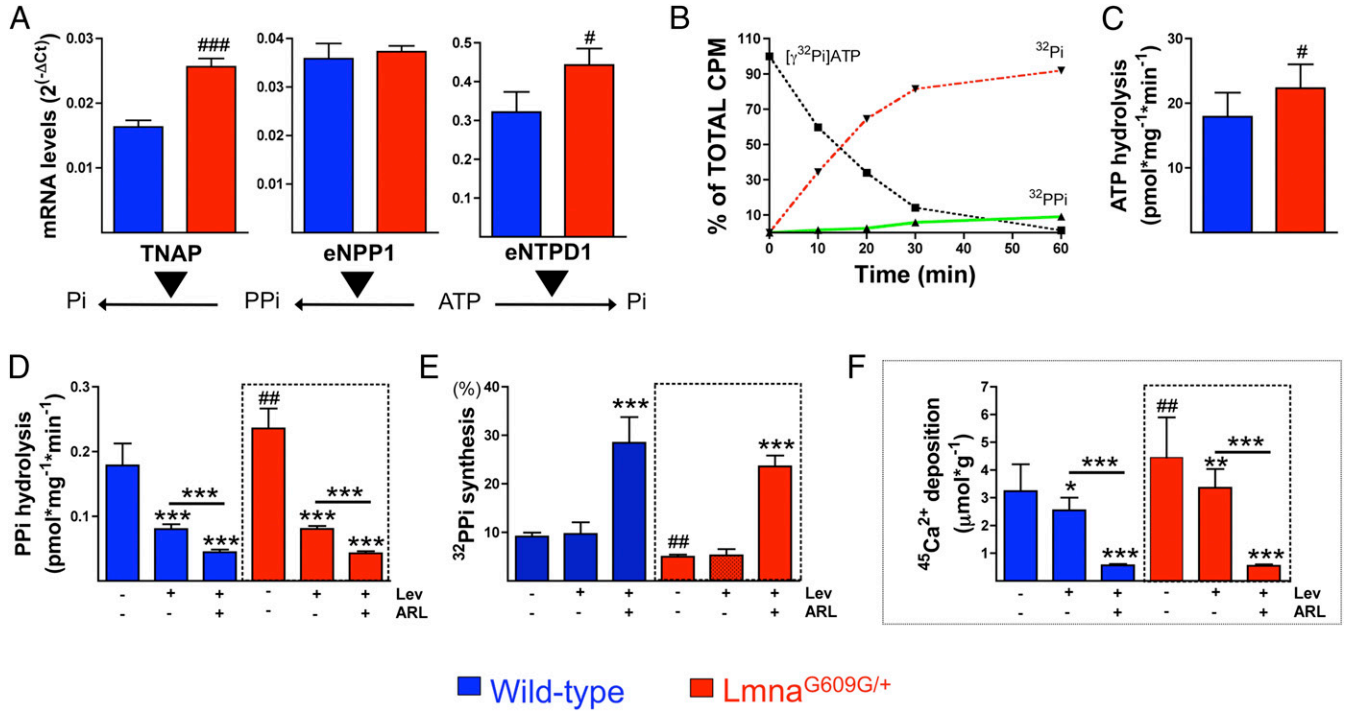

Fig. 1. eNTPD is the main activity in the aorta. (*A*) Levels of eNTPD1, eNPP1, and TNAP mRNAs in aortas of 30–32-wk-old wild-type and *Lmna*$^{G609G/+}$ mice ($n = 8$ aorta pools). (*B*) ^{32}PPi (32-pyrophosphate) and ^{32}Pi (32-phosphate) produced by hydrolysis of 1 μmol/L ATP containing 10 μCi/mL [γ^{32}P]ATP as a radiotracer over the indicated times. ^{32}PPi, ^{32}Pi, and [γ^{32}P]ATP were separated by TLC, as described in the *Methods* section. (*C*) ATP hydrolysis in wild-type and *Lmna*$^{G609G/+}$ aortas, quantified as ^{32}Pi produced by 1 μmol/L ATP containing 10 μCi/mL [γ^{32}P]ATP as a radiotracer after incubation for 5 and 10 min ($n = 21$). The mean of 2 timepoints is shown. (*D*) Pyrophosphate (PPi) hydrolysis in wild-type and *Lmna*$^{G609G/+}$ aortas, quantified as ^{32}Pi released by hydrolysis of 1 μmol/L pyrophosphate containing 10 μCi/mL ^{32}PPi as a radiotracer after incubation for 2 and 4 h ($n = 21$). The mean of 2 timepoints is shown. (*E*) ^{32}PPi produced by the hydrolysis of 1 μmol/L ATP containing 10 μCi/mL [γ^{32}P]ATP after incubation for 100 min in the absence or presence of 200 μmol/L levamisole (+Lev) or ARL67156 (+ARL). ^{32}PPi (*E*) and ^{32}Pi (*C* and *D*) production was quantified using the isobutanol/petroleum extraction method. (*F*) Forty-five-calcium accumulation in wild-type and *Lmna*$^{G609G/+}$ aortas ex vivo. Statistical analyses by 1-way ANOVA and Tukey's multiple comparisons posttest or Student's *t* test (in *C*). $^{\#}P < 0.05$; $^{\#\#}P < 0.01$; $^{\#\#\#}P < 0.001$, compared with wild-type control (no inhibitors). $^{**}P < 0.01$; $^{***}P < 0.001$, compared with control (no inhibitors).

Quantification of Aortic Calcium. Mouse aortas were dried, weighed, and treated with 0.6 mol/L HCl for 24 h. Calcium was quantified using a colorimetric QuantiChrom calcium assay kit (BioAssay Systems).

Mitochondrial Assays. Mitochondrial ATP synthesis was measured by kinetic luminescence assay (20). Cytochrome *c* oxidase (COX) and citrate synthase (CS) enzymatic activities were measured as described previously (20). COX activity was normalized to CS, a Krebs cycle enzyme used as an index of mitochondrial mass.

ATP and Pyrophosphate Quantification. Blood was obtained from 30 to 32-wk-old mice in heparin-containing tubes. Plasma was separated from cell components by centrifugation (5000 × g for 10 min, 4 °C). Plasma was frozen in liquid nitrogen and stored in −80 °C. Extracellular pyrophosphate was measured with an enzyme-linked bioluminescence assay as described previously (20). ATP was measured by a coupled luciferin/luciferase reaction with an ATP determination kit (Invitrogen), as described previously (20).

Statistical Analysis. Results are presented as mean ± SD. The Kolmogorov-Smirnov test was used to assess the normality of the data. Student's *t* test or 1-way ANOVA and Tukey's multiple comparison posttest were used for statistical analyses. Longevity was assessed by the Kaplan-Meier method. All statistical analyses were performed using GraphPad Prism 5 software.

Data Availability. The data that support the findings of this study are available in figshare, reference number 10.6084/m9.figshare.9978794.

Results

Pyrophosphate Availability in Vascular Smooth Muscle Cells (VSMCs) Depends on the eNTPD1/eNPP1 Ratio. The contribution of the 3 main enzymes involved in extracellular pyrophosphate metabolism was analyzed in primary vascular smooth muscle cells (VSMCs) obtained from 30 to 32-wk-old *Lmna*$^{G609G/+}$ mice. Pyrophosphate production from hydrolysis of 1 μmol/L ATP was significantly reduced by siRNA knockdown of eNPP1 and enhanced by siRNA knockdown of eNTPD1 (*SI Appendix*, Fig. S1*A*), indicating that the eNPP/eNTPD activity ratio plays a key role in pyrophosphate synthesis. By contrast, pyrophosphate production from ATP hydrolysis was unaffected by siRNA knockdown of TNAP, despite this knockdown significantly reducing pyrophosphate hydrolysis (*SI Appendix*, Fig. S1*B*). Moreover, calcium accumulation in VSMCs was significantly increased by siRNA knockdown of eNPP1 (*SI Appendix*, Fig. S1*C*) but was significantly reduced by siRNA knockdown of TNAP ($P < 0.05$) and eNTPD1 ($P < 0.001$).

Combination of TNAP/eNTPD Inhibitors Improved Pyrophosphate Availably in *Lmna*$^{G609G/+}$ VSMCs. Combination of TNAP inhibitor levamisole and the eNTPD inhibitor ARL67156 increased extracellular pyrophosphate synthesis in *Lmna*$^{G609G/+}$ VSMCs 2-fold (*SI Appendix*, Fig. S1*D*). By contrast, ARL67156 plus levamisole reduced extracellular pyrophosphate hydrolysis in *Lmna*$^{G609G/+}$ VSMCs by 91% (*SI Appendix*, Fig. S1*E*). Finally, the addition of levamisole and ARL67156 reduced calcium accumulation by 92% in *Lmna*$^{G609G/+}$ VSMCs (*SI Appendix*, Fig. S1*F*).

eNTPD Is the Main Activity in Aorta. To assess aortic calcification in HGPS mice, extracellular pyrophosphate metabolism was examined in *Lmna*$^{G609G/+}$ and wild-type mouse aortas. In wild-type aortas, the eNTPD1 mRNA level was 20- and 9-fold higher than eNPP1 and TNAP mRNA levels, respectively (Fig. 1*A*). Compared with the wild type, TNAP and eNTPD1 mRNA levels in *Lmna*$^{G609G/+}$ aortas were increased by 57% and 38%, respectively.

Aortas ex vivo completely hydrolyzed 1 μmol/L ATP after 60 min. TLC of wild-type hydrolysis products of [γ^{32}P]ATP resulted in a 9% yield of pyrophosphate (Fig. 1*B*), showing that eNTPD activity (ATP → phosphate) was greater than eNPP activity (ATP → pyrophosphate).

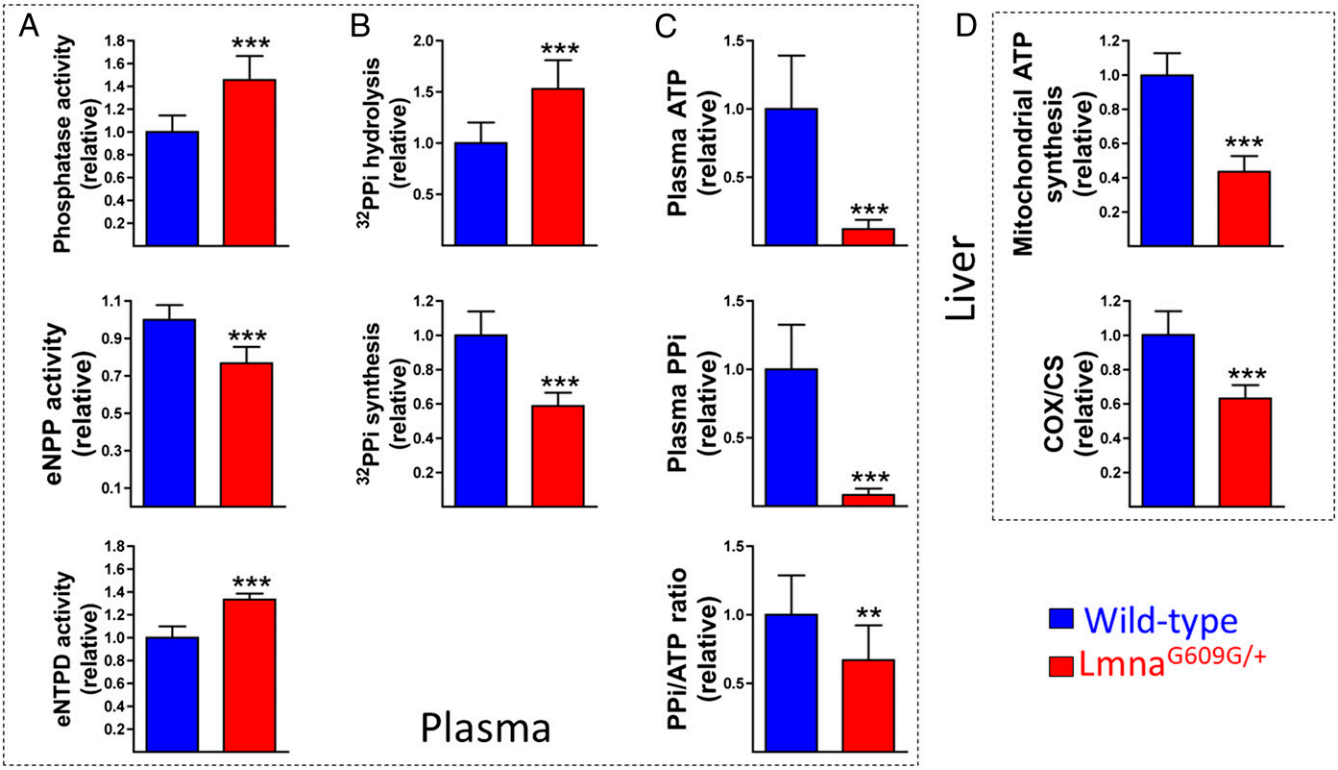

Fig. 2. Loss of systemic pyrophosphate synthesis. (*A*) Plasma phosphatase, eNPP, and eNTPD activities in 30–32-wk-old wild-type and *Lmna*$^{G609G/+}$ mice. (*B*) Pyrophosphate synthesis and hydrolysis in plasma. (*C*) Plasma ATP, pyrophosphate, and pyrophosphate/ATP ratio. (*D*) Mitochondrial ATP synthesis and COX:CS ratio in liver. Statistical analyses by Student's *t* test. $^{**}P < 0.01$; $^{***}P < 0.001$.

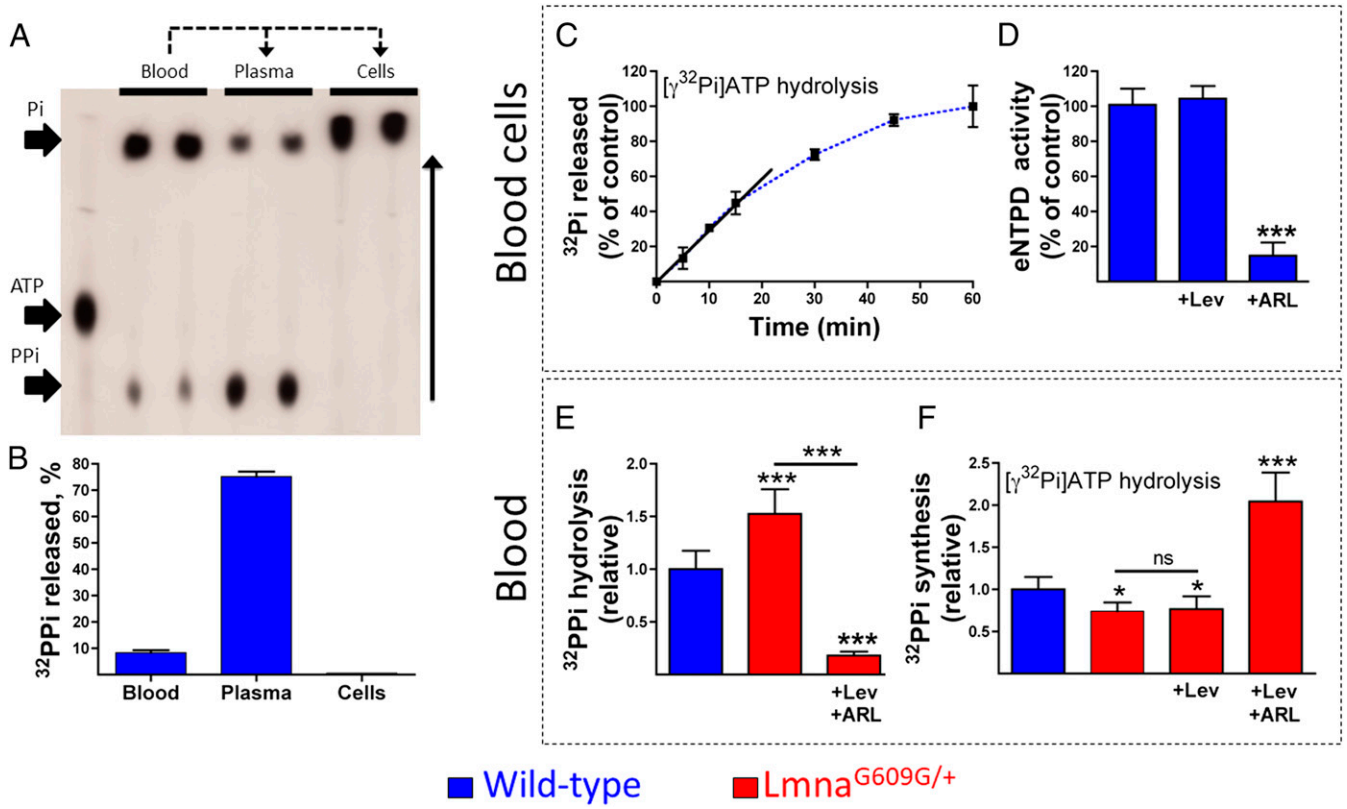

Fig. 3. eNTPD is the main activity in blood. (*A*) Representative autoradiograph showing the products released by incubation of 1 μmol/L ATP containing 10 μCi/mL [γ^{32}P]ATP for 60 min with blood, plasma, or blood cell components. ^{32}PPi (32-pyrophosphate), ^{32}Pi (32-phosphate), and [γ^{32}P]ATP were separated by TLC, as described in the *Methods* section. (*B*) ^{32}PPi released after 60 min of incubation with 1 μmol/L ATP containing 10 μCi/mL [γ^{32}P]ATP. ^{32}PPi was quantified using the isobutanol/petroleum extraction method (n = 12). (*C*) ^{32}Pi produced by incubation of 1 μmol/L ATP containing 10 μCi/mL [γ^{32}P]ATP over the indicated times in blood cells obtained from *Lmna*$^{G609G/+}$ mice. ^{32}Pi was quantified using the isobutanol/petroleum extraction method. (*D*) eNTPD activity of *Lmna*$^{G609G/+}$ blood cells in the absence or presence of 200 μmol/L levamisole (+Lev) or ARL67156 (+ARL) (n = 12). (*E*) ^{32}PPi hydrolysis in blood samples of wild-type and *Lmna*$^{G609G/+}$ mice in the absence or presence of levamisole (+Lev) and ARL67156 (+ARL). (*F*) ^{32}PPi produced by the hydrolysis of 1 μmol/L ATP containing 10 μCi/mL [γ^{32}P]ATP after 60 min of incubation in blood samples of wild-type and *Lmna*$^{G609G/+}$ mice in the absence or presence of levamisole and ARL67156 (n = 18). Statistical analyses by 1-way ANOVA and Tukey's multiple comparison posttests. *P < 0.05; ***P < 0.001; ns, nonsignificant difference.

ATP hydrolysis (Fig. 1*C*) was 101-fold faster than pyrophosphate hydrolysis (Fig. 1*D*) in wild-type ex vivo aortas (17.9 ± 3.74 versus 0.18 ± 0.03 pmol*mg^{-1}*min^{-1}). Compared with wild-type aortas, extracellular ATP and pyrophosphate hydrolysis were increased by 25% (to 22.3 ± 3.71 pmol*mg^{-1}*min^{-1}) and 32% (to 0.24 ± 0.03 pmol*mg^{-1}*min^{-1}), respectively, in Lmna$^{G609G/+}$ aortas. Incubation with levamisole, a TNAP inhibitor, reduced extracellular pyrophosphate hydrolysis in wild-type and *Lmna*$^{G609G/+}$ aortas by 55% (to 80.2 ± 7.5 fmol*mg^{-1}*min^{-1}) and 66% (to 80.4 ± 4.5 fmol*mg^{-1}*min^{-1}), respectively. Moreover, the combination of levamisole and the eNTPD inhibitor ARL67156 reduced extracellular pyrophosphate hydrolysis in wild-type and *Lmna*$^{G609G/+}$ aortas by 75% (to 44.3 ± 4.1 fmol*mg^{-1}*min^{-1}) and 82% (to 42.5 ± 3.4 fmol*mg^{-1}*min^{-1}), respectively. These findings indicated that TNAP mainly hydrolyzed extracellular pyrophosphate in normal aortas, with the residual extracellular pyrophosphate hydrolysis due to eNTPD activity (11).

Extracellular pyrophosphate synthesis was 46% lower in *Lmna*$^{G609G/+}$ than in wild-type aortas (5 ± 0.4% versus 9.2 ± 0.8%; Fig. 1*E*). The addition of levamisole had no effect on extracellular pyrophosphate synthesis, as shown in rat aortic rings (17). By contrast, ARL67156 plus levamisole increased extracellular pyrophosphate synthesis in wild-type and *Lmna*$^{G609G/+}$ aortas 3.1-fold (to 28.5 ± 5.3%) and 4.7-fold (to 23.6 ± 2.2%), respectively.

Calcium accumulation was 30% higher in *Lmna*$^{G609G/+}$ than in wild-type aortas cultured ex vivo (4.24 ± 1.16 versus 3.23 ± 0.97 μmol calcium*g^{-1}; Fig. 1*F*). The addition of levamisole and ARL67156 reduced calcium accumulation by 83% and 87% in wild-type and *Lmna*$^{G609G/+}$ aortas, respectively, whereas the addition of levamisole alone reduced calcium accumulation by 24% and 22%, respectively. This result indicated that calcification of *Lmna*$^{G609G/+}$ aortas was incremental and was due to alterations in extracellular pyrophosphate metabolism, resulting in deficient pyrophosphate synthesis. Moreover, these findings showed that a combination of eNTPD and TNAP inhibitors reduced vascular calcification ex vivo.

Loss of Systemic Pyrophosphate Synthesis. Systemic extracellular pyrophosphate was analyzed in HGPS mice using blood from Lmna$^{G609G/+}$ and wild-type mice. Plasma phosphatase and eNTPD activities were 46% and 33% higher, respectively, whereas eNPP activity was 23% lower, in *Lmna*$^{G609G/+}$ than in wild-type mice (Fig. 2*A*). In addition, extracellular pyrophosphate hydrolysis was 53% higher while extracellular pyrophosphate synthesis was 41% lower in plasma of *Lmna*$^{G609G/+}$ than of wild-type mice (Fig. 2*B*).

Plasma ATP and pyrophosphate concentrations were 88% and 92% lower, respectively, in *Lmna*$^{G609G/+}$ than in wild-type mice (Fig. 2*C*). However, the plasma pyrophosphate/ATP ratio was also 33% lower in *Lmna*$^{G609G/+}$ than in the wild type, indicating that extracellular pyrophosphate resulting from the hydrolysis of

ATP was reduced. The liver is the main source of extracellular ATP in plasma (21, 22). Mitochondrial synthesis and the COX:CS ratio were 57% and 37% lower, respectively, in livers of *Lmna*$^{G609G/+}$ mice (Fig. 2*D*), indicating that mitochondrial ATP synthesis was impaired in the liver. This impairment was associated with a significantly lower COX:CS ratio, indicating that the activity of COX, an essential component of the mitochondrial electron transport chain, was also impaired (20).

eNTPD Is the Main Activity in Blood. Incubation of blood samples from both types of mice completely hydrolyzed ATP after 1 h (Fig. 3*A*). Blood incubated with ATP produced 8.4% pyrophosphate (Fig. 3*B*), indicating that, as in aortas, eNTPD (ATP → phosphate) is the main activity in blood. However, pyrophosphate synthesis in plasma was 75% higher, indicating that eNPP activity (ATP → pyrophosphate) was predominant. By contrast, ATP hydrolysis by blood cell components (containing erythrocytes and leukocytes) produced phosphate (Fig. 3 *A*–*C*), which was reduced to 15% by the addition of the eNTPD inhibitor ARL67156, but was unaffected by levamisole (Fig. 3*D*). These findings indicated that eNPP and eNTPD activities are mainly located in plasma and blood cell components, respectively. Notably, eNTPD activity has been previously detected both in erythrocytes (23) and leukocytes, including monocytes, neutrophils, and lymphocytes (24).

Pyrophosphate hydrolysis was 52.5% higher (Fig. 3*E*), whereas pyrophosphate production by ATP hydrolysis was 26% lower in *Lmna*$^{G609G/+}$ than in wild-type blood (Fig. 3*F*). The addition of eNTPD and TNAP inhibitors reduced pyrophosphate hydrolysis by 82%, while increasing pyrophosphate production by 2.1-fold, in *Lmna*$^{G609G/+}$ blood. By contrast, levamisole had no effect on pyrophosphate production (Fig. 3*F*).

ATP-Based Therapy Improved Calcification and Longevity in *Lmna*$^{G609G/+}$ Mice. To assess the effects of ATP replacement therapy alone or in combination with eNTPD and TNAP inhibitors, 8-wk-old *Lmna*$^{G609G/+}$ mice were intraperitoneally injected with these compounds. Compared with untreated *Lmna*$^{G609G/+}$ mice, ATP alone did not significantly affect life span (38.2 versus 38.9 wk; $P = 0.225$; Fig. 4*A*) or total body weight (23.1 ± 1.8 versus 23.4 ± 0.9 wk; $P = 0.436$; Fig. 4*B*), but significantly reduced the calcium content in aortas of 34-wk-old mice (837.4 ± 189.7 versus 561.2 ± 121.7 μg/g; $P < 0.01$; Fig. 4*C*). Treatment with ATP, levamisole, and ARL67156 significantly increased life span from 38.2 to 42.8 wk (11.9%, $P < 0.001$; Fig. 4*A*) and total body weight from 23.1 ± 1.8 g to 25.8 ± 1.0 g ($P < 0.001$; Fig. 4 *B* and *D*), while significantly reducing calcium in the aorta from 837.4 ± 189.7–443.9 ± 76.3 μg/g ($P < 0.001$; Fig. 4*C*).

Discussion

Hutchinson–Gilford progeria syndrome is caused by the accumulation at the nuclear envelope of the farnesylated form of truncated prelamin A, a protein that is altered during normal aging (6, 7). Most people with HGPS have a single nucleotide substitution within exon 11 of the gene encoding lamin A (LMNA). This mutation (GGC → GGT; G608G) activates a cryptic splice-donor site, finally leading to a truncated, permanently farnesylated prelamin A isoform, which induces a dimorphic nuclear phenotype in HGPS patients (6, 7).

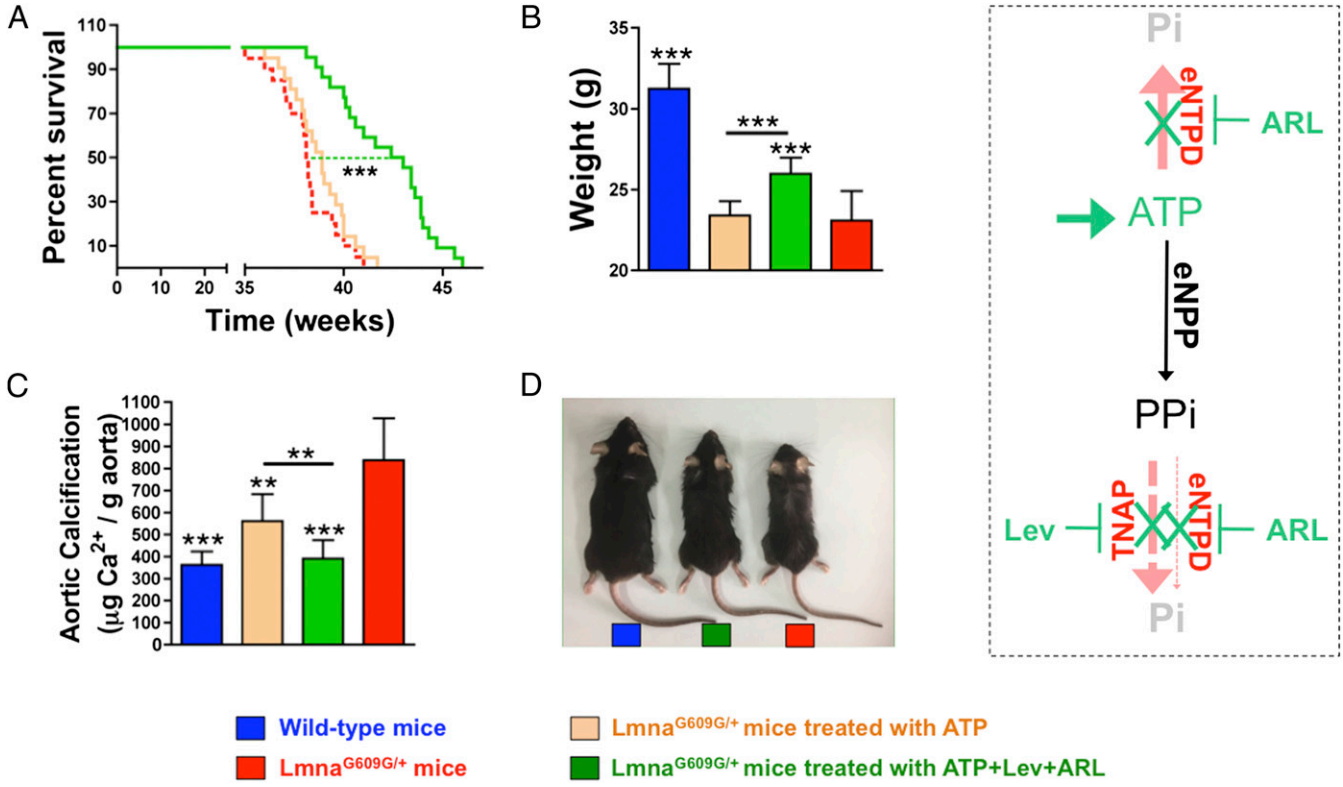

Fig. 4. ATP-based therapy improved calcification and longevity in *Lmna*$^{G609G/+}$ mice. (*A*) Kaplan-Meier graph of the survival of *Lmna*$^{G609G/+}$ mice ($n = 20$) and *Lmna*$^{G609G/+}$ mice treated with ATP ($n = 21$) or with a combination of ATP, levamisole (Lev) and ARL67156 (ARL) ($n = 22$). (*B*) Total body weight of 34-wk-old wild-type mice, *Lmna*$^{G609G/+}$ mice, and *Lmna*$^{G609G/+}$ mice treated with ATP or with a combination of ATP, Lev, and ARL. (*C*) Calcium content in aortas obtained from 34-wk-old wild-type mice ($n = 22$), *Lmna*$^{G609G/+}$ mice ($n = 22$), and *Lmna*$^{G609G/+}$ mice treated with ATP ($n = 19$) or with ATP+Lev+ARL ($n = 17$). (*D*) Representative photographs of 38-wk-old wild-type mice, *Lmna*$^{G609G/+}$ mice, and *Lmna*$^{G609G/+}$ mice treated with a combination of ATP, Lev, and ARL. Statistical analyses by 1-way ANOVA and Tukey's multiple comparison posttests. $^{**}P < 0.01$; $^{***}P < 0.001$ compared with untreated *Lmna*$^{G609G/+}$ mice.

The first treatment strategy for HGPS was based on the ability of farnesyl transferase inhibitors (FTIs) to reverse the nuclear phenotype (25). However, prelamin A and progerin undergo alternative prenylation by geranylgeranyl transferase when farnesyl transferase activity is inhibited. For this reason, an alternative treatment strategy employed a combination of statins and bisphosphonates, inhibitors of HMG-CoA reductase, and farnesyl-PP synthase, respectively, to inhibit efficiently both farnesylation and geranylgeranylation of progerin and prelaminar, which markedly improved the aging-like phenotypes of progeroid mice, including weight loss and decreased longevity (26). These treatments showed less efficiency in children with HGPS (27, 28).

The second HGPS treatment strategy was based on reversion of the HGPS mutation using CRISP-Cas9, which extended longevity in HGPS mice (29, 30). However, this treatment is still far from being applicable in humans.

This study herein presents an alternative strategy for the treatment of HGPS. Like in humans, HGPS mice display excessive vascular calcification as a consequence of a reduced level of extracellular pyrophosphate, a potent endogenous inhibitor of calcification (10, 20). Our study shown herein that this reduction in extracellular pyrophosphate levels in HGPS mice is a consequence of the impaired synthesis of pyrophosphate both in the aorta and blood, which in turn is caused by several factors including 1) the up-regulation of the ectoenzymes TNAP (the main enzyme involved in pyrophosphate degradation) and eNTPD1 (an enzyme that hydrolyzes ATP to release phosphate), and 2) reduced ATP production (the source of pyrophosphate) caused by mitochondrial dysfunction associated with reduced complex IV COX activity. Vascular calcification is dependent mainly on plasma levels of pyrophosphate (10). However, as a main source of pyrophosphate, ATP plays a key role in preventing vascular calcification (31). Moreover, ATP could also directly inhibit calcium deposition on the aortic wall (32). ATP availability is dramatically reduced in $Lmna^{G609G/+}$ mice. Increments in extracellular pyrophosphate degradation and reduction in extracellular pyrophosphate synthesis found in this study impair the availability of extracellular pyrophosphate in aorta and blood.

Notably, activity of eNTPD (ATP → phosphate) is predominant and it hydrolyzes more than 90% of ATP in the aorta and blood. Therefore, eNPP (ATP → pyrophosphate) hydrolyzes less than 10% of ATP to form pyrophosphate. Inhibition of eNTPD and TNAP activity reduced pyrophosphate hydrolysis in both $Lmna^{G609G/+}$ aortas and blood, as well as increasing pyrophosphate synthesis through ATP hydrolysis, indicating that alterations in the eNPP/eNTPD activity ratio via eNTPD inhibition were more effective than inhibition of TNAP activity in increasing extracellular pyrophosphate availability. Moreover, the combination of eNTPD and TNAP inhibitors reduced calcification in aortas ex vivo, whereas pyrophosphate degradation during ex vivo pyrophosphate production by ATP hydrolysis was negligible, suggesting that long-term studies are required to assess the effect of phosphatase activity on extracellular pyrophosphate availability.

Finally, combined treatment in HGPS mice with ATP and inhibitors of TNAP and eNTPD resulted in extension of longevity and the prevention of vascular calcification, a common clinical manifestation also associated with aging, diabetes, and chronic kidney disease. Moreover, combined treatment with ATP and TNAP/eNTPD inhibitors may also increase the availability of ATP in local tissue and provide more energy for maintenance of life. Therefore, this HGPS treatment strategy, focused on improving extracellular ATP/pyrophosphate metabolism, could constitute an alternative therapy against this devastating syndrome.

This study also showed that the eNPP/eNTPD activity ratio plays a key role in pyrophosphate availability, as this ratio could determine the ratio of pyrophosphate/phosphate synthesis from ATP. By altering the eNPP/eNTPD activity ratio, eNTPD inhibitors lead to increments in pyrophosphate availability. ATP replacement therapy, combined with TNAP and eNTPD inhibitors, may provide an alternative to eNPP replacement therapy (33) in patients with HGPS or other diseases with pyrophosphate deficiency, such as *Pseudoxanthoma elasticum* (34).

ACKNOWLEDGMENTS. I thank Daniel Azpiazu, Ana Lobo, Ana de la Calle, Veronica, and Jose Luis for excellent technical assistance. I also thank personnel of FIIS-FJD Animal Facility for animal production and maintenance. This study was supported by grants from Progeria Research Foundation (PRF-2016-68) from the United States and Spanish Ministerio de Economía y Competitividad (MINECO)(SAF-2014-60669-JIN).

1. K. Nair, P. Ramachandran, K. M. Krishnamoorthy, S. Dora, T. J. Achuthan, Hutchinson-Gilford progeria syndrome with severe calcific aortic valve stenosis and calcific mitral valve. *J. Heart Valve Dis.* **13**, 866–869 (2004).
2. M. Salamat, P. K. Dhar, D. L. Neagu, J. B. Lyon, Aortic calcification in a patient with hutchinson-gilford progeria syndrome. *Pediatr. Cardiol.* **31**, 925–926 (2010).
3. N. B. Hanumanthappa, G. Madhusudan, J. Mahimarangaiah, C. N. Manjunath, Hutchinson-Gilford progeria syndrome with severe calcific aortic valve stenosis. *Ann. Pediatr. Cardiol.* **4**, 204–206 (2011).
4. M. R. Hamczyk *et al*., Vascular smooth muscle-specific progerin expression accelerates atherosclerosis and death in a mouse model of Hutchinson-Gilford progeria syndrome. *Circulation* **138**, 266–282 (2018).
5. M. A. Merideth *et al*., Phenotype and course of Hutchinson-Gilford progeria syndrome. *N. Engl. J. Med.* **358**, 592–604 (2008).
6. A. De Sandre-Giovannoli *et al*., Lamin a truncation in Hutchinson-Gilford progeria. *Science* **300**, 2055 (2003).
7. M. Eriksson *et al*., Recurrent de novo point mutations in lamin A cause Hutchinson-Gilford progeria syndrome. *Nature* **423**, 293–298 (2003).
8. F. G. Osorio *et al*., Splicing-directed therapy in a new mouse model of human accelerated aging. *Sci. Transl. Med.* **3**, 106ra107 (2011).
9. R. Villa-Bellosta, W. C. O'Neill, Pyrophosphate deficiency in vascular calcification. *Kidney Int.* **93**, 1293–1297 (2018).
10. K. A. Lomashvili, S. Narisawa, J. L. Millán, W. C. O'Neill, Vascular calcification is dependent on plasma levels of pyrophosphate. *Kidney Int.* **85**, 1351–1356 (2014).
11. R. Villa-Bellosta, X. Wang, J. L. Millán, G. R. Dubyak, W. C. O'Neill, Extracellular pyrophosphate metabolism and calcification in vascular smooth muscle. *Am. J. Physiol. Heart Circ. Physiol.* **301**, H61–H68 (2011).
12. C. R. Sheen *et al*., Pathophysiological role of vascular smooth muscle alkaline phosphatase in medial artery calcification. *J. Bone Miner. Res.* **30**, 824–836 (2015).
13. S. Narisawa *et al*., Novel inhibitors of alkaline phosphatase suppress vascular smooth muscle cell calcification. *J. Bone Miner. Res.* **22**, 1700–1710 (2007).
14. S. G. Ziegler *et al*., Ectopic calcification in pseudoxanthoma elasticum responds to inhibition of tissue-nonspecific alkaline phosphatase. *Sci. Transl. Med.* **9**, eaal1669 (2017).
15. F. Rutsch *et al*., Mutations in ENPP1 are associated with 'idiopathic' infantile arterial calcification. *Nat. Genet.* **34**, 379–381 (2003).
16. K. Johnson, M. Polewski, D. van Etten, R. Terkeltaub, Chondrogenesis mediated by PPi depletion promotes spontaneous aortic calcification in NPP1-/- mice. *Arterioscler. Thromb. Vasc. Biol.* **25**, 686–691 (2005).
17. R. Villa-Bellosta, Synthesis of extracellular pyrophosphate increases in vascular smooth muscle cells during phosphate-induced calcification. *Arterioscler. Thromb. Vasc. Biol.* **38**, 2137–2147 (2018).
18. R. Villa-Bellosta, M. R. Hamczyk, Isolation and culture of aortic smooth muscle cells and in vitro calcification assay. *Methods Mol. Biol.* **1339**, 119–129 (2015).
19. R. Villa-Bellosta, Impact of magnesium:calcium ratio on calcification of the aortic wall. *PLoS One* **12**, e0178872 (2017).
20. R. Villa-Bellosta *et al*., Defective extracellular pyrophosphate metabolism promotes vascular calcification in a mouse model of Hutchinson-Gilford progeria syndrome that is ameliorated on pyrophosphate treatment. *Circulation* **127**, 2442–2451 (2013).
21. R. S. Jansen *et al*., ABCC6-mediated ATP secretion by the liver is the main source of the mineralization inhibitor inorganic pyrophosphate in the systemic circulation-brief report. *Arterioscler. Thromb. Vasc. Biol.* **34**, 1985–1989 (2014).
22. R. S. Jansen *et al*., ABCC6 prevents ectopic mineralization seen in pseudoxanthoma elasticum by inducing cellular nucleotide release. *Proc. Natl. Acad. Sci. U.S.A.* **110**, 20206–20211 (2013).
23. N. Montalbetti *et al*., Homeostasis of extracellular ATP in human erythrocytes. *J. Biol. Chem.* **286**, 38397–38407 (2011).
24. E. D. Pulte *et al*., CD39/NTPDase-1 activity and expression in normal leukocytes. *Thromb. Res.* **121**, 309–317 (2007).
25. B. C. Capell *et al*., Inhibiting farnesylation of progerin prevents the characteristic nuclear blebbing of Hutchinson-Gilford progeria syndrome. *Proc. Natl. Acad. Sci. U.S.A.* **102**, 12879–12884 (2005).

26. I. Varela *et al*., Combined treatment with statins and aminobisphosphonates extends longevity in a mouse model of human premature aging. *Nat. Med.* **14**, 767–772 (2008).
27. L. B. Gordon *et al*., Clinical trial of the protein farnesylation inhibitors lonafarnib, pravastatin, and zoledronic acid in children with Hutchinson-Gilford progeria syndrome. *Circulation* **134**, 114–125 (2016).
28. L. B. Gordon *et al*., Clinical trial of a farnesyltransferase inhibitor in children with Hutchinson-Gilford progeria syndrome. *Proc. Natl. Acad. Sci. U.S.A.* **109**, 16666–16671 (2012).
29. O. Santiago-Fernández *et al*., Development of a CRISPR/Cas9-based therapy for Hutchinson-Gilford progeria syndrome. *Nat. Med.* **25**, 423–426 (2019).
30. E. Beyret *et al*., Single-dose CRISPR-Cas9 therapy extends lifespan of mice with Hutchinson-Gilford progeria syndrome. *Nat. Med.* **25**, 419–422 (2019).
31. R. Villa-Bellosta, On vascular calcification and plasma levels of pyrophosphate. *Kidney Int.* **87**, 239 (2015).
32. R. Villa-Bellosta, V. Sorribas, Prevention of vascular calcification by polyphosphates and nucleotides- role of ATP. *Circ. J.* **77**, 2145–2151 (2013).
33. R. A. Albright *et al*., ENPP1-Fc prevents mortality and vascular calcifications in rodent model of generalized arterial calcification of infancy. *Nat. Commun.* **6**, 10006 (2015).
34. M. Dabisch-Ruthe, P. Kuzaj, C. Götting, C. Knabbe, D. Hendig, Pyrophosphates as a major inhibitor of matrix calcification in Pseudoxanthoma elasticum. *J. Dermatol. Sci.* **75**, 109–120 (2014).